

## Turbulent Drag Reduction Using an Array of Piezo-ceramic Actuators

W. G. Zhang<sup>1,2</sup>, Y. Zhou<sup>1</sup> and H. L. Bai<sup>1</sup>

<sup>1</sup>Department of Mechanical Engineering  
The Hong Kong Polytechnic University, Hung Hom, Kowloon, Hong Kong SAR, P. R. China

<sup>2</sup>China Aerodynamic Research & Development Center  
P. O. Box 211, Mianyang, Sichuan 621000, P. R. China

### Abstract

An experimental investigation on active control of turbulent boundary layer (TBL), aiming at reducing skin-friction drag, has been conducted in a wind tunnel at  $Re_\theta = 1,000$ , based on the free-stream velocity ( $U_\infty$ ) and momentum thickness ( $\theta$ ). A spanwise-aligned piezo-ceramic (PZT) actuator array, consisting of 16 elements, was employed to generate wall-normal oscillations and, given a phase shift between two adjacent actuators, a transverse travelling wave along the wall surface. A wide range of parameters were examined, including the wavelength (41.6 ~  $\infty$  wall units), oscillation frequency (0.13 ~ 0.65 wall units) and amplitude (0.83 ~ 2.77 wall units). Local skin-friction drag can be reduced as much as 50% at a location of 17 wall units downstream of the actuator tip, based on the change of hotwire-measured slope of mean streamwise velocity profile in the near-wall region, when the actuator array worked at a wavelength, oscillation amplitude and frequency of 416, 1.94 and 0.39, respectively, all in wall units. The near-wall flow structures with and without control were extensively measured using laser-illuminated smoke-wire flow visualization, hotwire and hot-film, and were compared with each other. Under the optimum control parameters, large-scale coherent structures were disturbed tremendously, resulting in comparatively steady small-scale structures. Moreover, results of two-point cross-correlation between wall shear stress and streamwise velocity reveal that near-wall shear layers were impaired significantly and pushed upward slightly, toward skin-friction drag reduction, during the perturbations.

### Introduction

Due to the necessity and urgency of energy saving, reducing skin-friction drag in a TBL has been highlighted recently. Various control techniques have been developed so far. Compared with passive control techniques, because of its drastic effect, active techniques have attracted a significantly increased attention in literatures [1].

Both experimental and numerical studies have indicated a close association between quasi-streamwise vortices (QSVs) and large wall shear stress [2-4]. The production of the mean Reynolds stress (subsequently viscous drag) is linked directly to the dynamics of QSVs in the near-wall region. QSVs are generally located immediately above and displaced laterally from high skin-friction-drag regions. The well-known turbulent events, i.e. ejection, burst and sweep, in a TBL are all related to QSVs. Both ejection and sweep are induced by the vortices. The sweep is responsible for the large skin-friction drag and is therefore particularly important for drag reduction [5].

Controlling QSVs in the near-wall region is the key of drag reduction techniques. Applying an open-loop-controlled oscillating spanwise Lorentz force to a channel flow, Berger et al.

(2000) [6] found that skin-friction drag could be reduced by 40%, though this control scheme was impractical because of a very low efficiency. A spanwise oscillating wall could reduce the skin-friction drag up to 45% [7], but the net energy saving is low due to the auxiliary mechanical movement. Recently, Du & Karniadakis (2000) [8] and Du et al. (2002) [9] investigated the effectiveness of transverse travelling wave, induced by a spanwise force, on drag reduction based on direct numerical simulation (DNS) data and observed a drag reduction exceeding 50% and meanwhile the significantly impaired near-wall streaks. Their preliminary experiments with Lorentz actuators and shape-memory alloys produced results consistent with the DNS data. Nevertheless, this technique has yet to be demonstrated experimentally [5].

The present work aims to investigate experimentally the skin-friction-drag reduction in a TBL using a PZT actuator array. The PZT-actuator array, consisting of 16 elements, was flush-mounted with the wall surface and aligned in the spanwise direction. Given a phase shift between two adjacent actuators, the actuator array can generate a transverse travelling wave along the wall. A wide range of parameters will be examined, including the wavelength, oscillation frequency and amplitude, with the local skin-friction drag downstream of the actuator array measured. The near-wall flow structures under control are measured, with the aid of smoke-wire flow visualization, hotwire and hot-film techniques, and are compared to that without control. Experimental details are given in the next section, followed by the section of results and discussions. This work is concluded briefly in the last section.

### Experimental Details

This investigation was carried out in a low-speed closed-circuit wind tunnel of 2.4 m  $\times$  0.6 m  $\times$  0.6 m. A flat plate, which was placed horizontally in the test section of the tunnel, was used to produce a boundary layer. The plate was slightly inclined to ensure a zero-pressure gradient along the test section. The boundary layer was tripped in the leading edge of the plate. Measurements were mostly performed at a free-stream velocity  $U_\infty = 2.4$  m/s, with the free-stream turbulent intensity of 0.7% in the presence of the plate. One array of PZT actuators was placed at 1.5 m downstream of the leading edge of the plate. At this downstream position the boundary layer was confirmed to be fully developed and, in the absence of actuation, the Reynolds number is  $Re_\theta = 1,000$ .

Figure 1 shows schematically the array of actuators, a total of 16 elements. Each element, flush-mounted with the plate surface, has a dimension of 22 mm  $\times$  2 mm  $\times$  0.33 mm (length  $\times$  width  $\times$  thickness). The actuators are cantilever-supported, with its inactive part (2 mm long) glued to a substrate, which is embedded in a circular plug-base. There is a cavity under each

actuator so that the active part (20 mm long) of the actuator can vibrate freely. The spanwise spacing between the actuators is 1 mm. As such, the entire actuator array spans 45 mm in the spanwise direction. The gap between the actuator and the wall edge around it is nominally 0.05 mm (refer to Details B in Figure 1). Each actuator was driven by an individual voltage amplifier and guaranteed to have the same peak-to-peak oscillation amplitude at the tip ( $A_o$ ) as others by adjusting its effective or root-mean-square (*rms*) driving voltage ( $V_o$ ) of a sinusoidal wave at each working frequency ( $f_o$ ) in a dSPACE control system (DS1006).  $A_o$  was measured using a laser vibrometer (Polytech OFV 3001 502). The phase shift ( $\phi_{i, i+1}$ ,  $i = 1, 2, \dots, 15$ ) between two adjacent actuators could be set and adjusted on the dSPACE control system. A discrete wave may be produced along the wall surface given a phase shift  $\phi_{i, i+1}$ . For instance, at  $\phi_{i, i+1} = 24^\circ$ , the 16 actuators form one discrete spanwise sinusoidal wave with a wavelength ( $\lambda_z$ ) of 45 mm. The origin of the coordinate system is at the actuator tip, with the  $x$ ,  $y$  and  $z$  axes along the streamwise, normal (to the wall) and spanwise (or transverse) directions, respectively. The arrangement of the 16 actuators is symmetric about the  $xy$ -plane at  $z = 0$ .

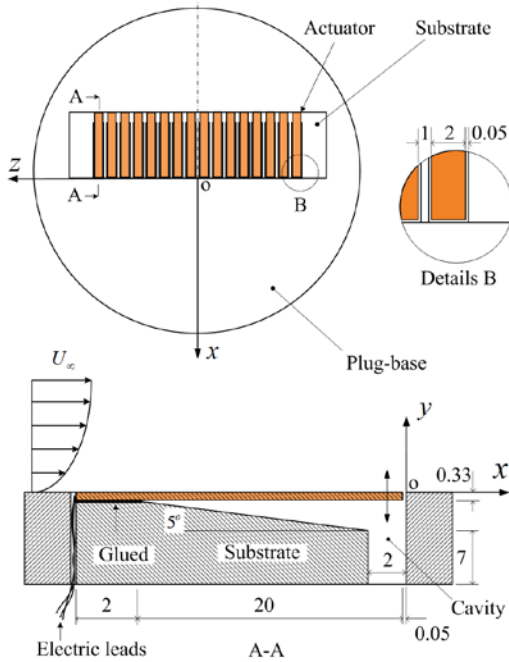


Figure 1. The schematic of experimental setup (not in scale, units in mm)

A miniature single-wire probe (55P15, Dantec), operated on a constant temperature anemometer (CTA, Dantec Streamline), was used to measure the instantaneous streamwise velocity  $U (= \bar{U} + u$ , where overbar denotes time-average and  $u$  is the fluctuating component) in the boundary layer and hence the wall-normal distribution of  $\bar{U}$ . The sensing element was a Tungsten wire of 5  $\mu\text{m}$  in diameter and about 1 mm in length, and was calibrated in the free stream using a Pitot-static tube. The hotwire probe was mounted on a computer-controlled three-dimensional (3D) traversing mechanism, whose resolution in the  $y$  direction is 10  $\mu\text{m}$ . An overheat ratio of 1.8 was used. The signal from the wire was offset, low-pass filtered at a cut-off frequency of 1.0 kHz, and then sampled at 2.5 kHz using a 16-bit A/D converter (Ni PCI-6143). The sampling duration for each record was 40 s, ensuring the *rms* value,  $u_{rms}$ , of  $u$  to be converged, within a 1% uncertainty.

The slope of  $\bar{U}$ -distribution in the linear region of the TBL was used to estimate the time-averaged wall shear stress,  $\bar{\tau}_w$ . Measurements were repeated five times, and the standard

deviation in the estimated  $\bar{\tau}_w$  is within  $\pm 2\%$ . It is observed that the linear behaviour of  $\bar{U}$ -distribution exists under control. Thus, the local skin-friction reduction is presently defined by  $\delta_{\tau_w} = [(\bar{\tau}_w)_{on} - (\bar{\tau}_w)_{off}] / (\bar{\tau}_w)_{off} \times 100\%$ , where  $(\bar{\tau}_w)_{on}$  and  $(\bar{\tau}_w)_{off}$  denote the time-averaged wall shear stress measured with and without control, respectively.

A hot-film probe (Dantec 55R45) was flush-mounted with the wall at  $z = 0$  and  $x = 5$  mm (or  $x^+ = 35$ , where '+' denotes normalization by wall variables) downstream of the actuator tip in order to measure the fluctuating component of  $\tau_w$ . Attached on the tip of a cylindrical quartz rod, the sensing element of the probe was a Nickel film, 0.2 mm longitudinally and 0.75 mm along the spanwise direction. The hot-film was operated on the CTA, with a setting similar to the hotwire operation. No calibration was performed.

The smoke-wire flow visualization was conducted in the  $xz$ -plane. A Nickel-Chrome wire of 0.1 mm in diameter, strained and supported on a fork attached to the 3D traversing mechanism, was placed at  $y^+ = 5$ , parallel to the wall surface and normal to the flow direction. The wire was painted with high-temperature-resistant paint for a length of 1.5 mm and a paint-free interval of 1 mm. Once heated by a direct current with a maximum of 30 mA from a tailor-made circuit, the wire covered with paraffin oil produces uniform smoke. Illumination was provided by a continuous laser light sheet of 0.8 mm thick in the  $xz$ -plane of  $y^+ = 6.5$ . The laser beam, guided through an optic fibre, was emitted from an argon ion laser source (Spectra-Physics) with a power output of 4 W and swept via a cylinder lens. A digital video camera (Sony DCR-PC100E) was used to record the flow field at a frame rate of 25 frames per section (fps).  $U_\infty$  was reduced to 1.5 m/s ( $Re_\theta = 650$ ) to capture the best flow visualization results. Normalization in smoke-wire flow visualization is based on wall variables at the lower  $U_\infty$ .

## Results and Discussions

### Dependence of Drag Reduction on Control Parameters

The spanwise travelling wave, formed by the 16 discrete actuators, depends on  $A_o^+$ ,  $f_o^+$ ,  $\lambda_z^+$  and  $\phi_{i, i+1}$ , where the latter two parameters are not independent of each other and specifying one gives another. All the parameters affect the change of local skin-friction drag,  $\delta_{\tau_w}$ . Figure 2(a) presents the dependence of  $\delta_{\tau_w}$ , measurement at  $x^+ = 35$  and  $z^+ = 0$ , on  $f_o^+$  given  $\lambda_z^+ = 416$  (or  $\phi_{i, i+1} = 18^\circ$ ) and  $A_o^+ = 1.11, 1.66, 1.94$  and  $2.22$ . At  $\lambda_z^+ = 416$ , the 16 actuators form one complete sinusoidal wave along the spanwise direction. At small  $A_o^+ = 1.11$ , about one-fifth of the viscous sub-layer thickness, the decrease in the friction drag is slow and insignificant from  $f_o^+ = 0.13$  to  $0.32$ , not more than 5%. However, the drop is appreciably accelerated for further increasing  $f_o^+$ , and then appears approaching its asymptotic values, about -15%, for  $f_o^+ > 0.58$ . At  $A_o^+ \geq 1.66$ , the friction drag is apparently more sensitive to  $f_o^+$ . With increasing  $f_o^+$ ,  $\delta_{\tau_w}$  declines, becoming more pronouncedly negative. This decline is rather rapid up to  $f_o^+ = 0.45$  for all the three  $A_o^+$ , and levels off for a further increase in  $f_o^+$ . The strong dependence of drag reduction on excitation frequency has also been observed in other control techniques such as a spanwise oscillatory Lorentz force [7] and a transverse travelling force wave [8, 9]. Presumably, the drag reduction under perturbation is connected to a change in QSVs and streaky structures in the near-wall region. The bursting frequency of near-wall events is estimated to be only  $f_b^+ = 0.0045$ , and then  $f_o^+ = 0.45$  is 100 times  $f_b^+$ . Segawa et al. (2002) [10] suggested that the reason of requiring higher  $f_o^+$  than  $f_b^+$  was ascribed to synchronization between the  $f_o^+$  and the duration of bursting process, instead of  $f_b^+$ .

The dependence of  $\delta_{\tau_w}$  on  $A_o^+$  is presented in Figure 2(b) given  $\lambda_z^+ = 416$ . Two different frequencies, i.e.  $f_o^+ = 0.39$  and  $0.65$ , were examined. At  $A_o^+ = 1.11$ , the friction drag reduction is no more than 10% for either  $f_o^+$ . However,  $\delta_{\tau_w}$  dips rapidly in both cases from  $A_o^+ = 1.11$  to  $1.94$ , where  $\delta_{\tau_w}$  reaches the minimum -30% for  $f_o^+ = 0.65$  or -35% for  $f_o^+ = 0.39$ , and climbs quickly for a further increase in  $A_o^+$ , in particular at the lower  $f_o^+$ . The observation is in agreement with Du et al.'s (2002) [9] finding based on the DNS data. In their study, a spatial transverse travelling wave was formed in terms of a spanwise force that was confined within the viscous sublayer. The force has the maximum on the wall and decayed exponentially away from it. They found that the largest drag reduction (more than 50%) was achieved when the penetration depth was about 10 wall units, comparable to the viscous sublayer thickness. Beyond this depth, the friction drag increased. Presumably, the disturbance to flow by the actuators has a correspondence to Du et al.'s (2002) [9] force penetration depth. It is then highly likely that the location which this disturbance reaches occurs at  $A_o^+ \approx 2$  is comparable to the viscous sublayer thickness, yielding the maximum drag reduction.

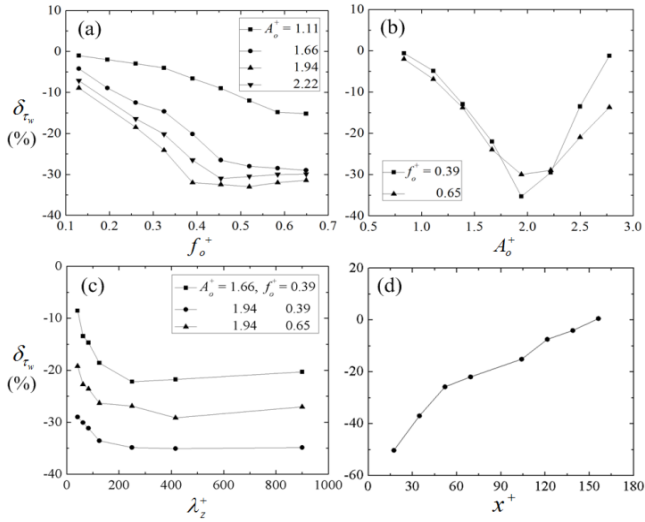


Figure 2. Dependence of normalized drag reduction  $\delta_{\tau_w}$  (%) on (a) oscillation frequency  $f_o^+$  ( $x^+ = 35, z^+ = 0, \lambda_z^+ = 416$ ), (b) magnitude  $A_o^+$  ( $x^+ = 35, z^+ = 0, \lambda_z^+ = 416$ ), (c) wavelength  $\lambda_z^+$  ( $x^+ = 35, z^+ = 0$ ), and (d) downstream measurement location  $x^+$  ( $z^+ = 0, A_o^+ = 1.94, f_o^+ = 0.39, \lambda_z^+ = 416$ ).

Variation in  $\lambda_z^+$  is realized by changing  $\phi_{i,i+1}$ . The dependence of  $\delta_{\tau_w}$  on  $\lambda_z^+$  is examined for three different combinations of  $A_o^+$  and  $f_o^+$ , i.e.  $(A_o^+, f_o^+) = (1.66, 0.39), (1.94, 0.39)$  and  $(1.94, 0.65)$ . From  $\lambda_z^+ = 42$  to  $125$ ,  $\delta_{\tau_w}$  declines quickly. However, beyond  $\lambda_z^+ = 125$ , the declination of  $\delta_{\tau_w}$  slows down and then approaches asymptotically a constant at  $\lambda_z^+ = \infty$ , regardless of the combination of  $A_o^+$  and  $f_o^+$ . Evidently, given a combination of  $A_o^+$  and  $f_o^+$ , drag reduction increases monotonically with increasing wavelength, which is qualitatively consistent with the observation of Du et al. (2002) [9]. Their numerical data support this trend at least within  $\lambda_z^+ = 840$ , which was the limitation of computation resource. One may note that discrete actuators are employed currently to form the transverse travelling wave; it is almost impossible to produce an ideal sinusoidal wave in the spanwise direction, as that has been done in numerical simulation. Furthermore, beyond  $\lambda_z^+ = 312$  (or  $\phi_{i,i+1} < 24^\circ$ ), the sinusoidal wave generated by the entire 16 PZT-actuators is incomplete. This may explain partially why the drag reduction declines quickly at  $\lambda_z^+ < 125$ , but slows down at  $\lambda_z^+ > 125$  with increasing  $\lambda_z^+$ .

One expects that  $\delta_{\tau_w}$  depends on  $x^+$  where  $\bar{\tau}_w$  is measured, which is indeed confirmed in Figure 2(d). The control parameters are  $A_o^+ = 1.94, f_o^+ = 0.39$  and  $\lambda_z^+ = 416$  ( $z^+ = 0$ ). At  $x^+ = 17$ , the friction drag reduction reaches more than 50%. As the measurement position was moved downstream from  $x^+ = 17$  to  $52$ , the friction drag reduction recovers rather rapidly and  $\delta_{\tau_w}$  climbs. Beyond  $x^+ = 52$ , this recovery slows down and  $\delta_{\tau_w}$  approaches zero at  $x^+ \approx 160$ .

### Altered Near-wall Flow Structures

The flow structure was examined, with more focus on the near-wall region, in order to gain insight into flow physics behind the observed drag reduction.

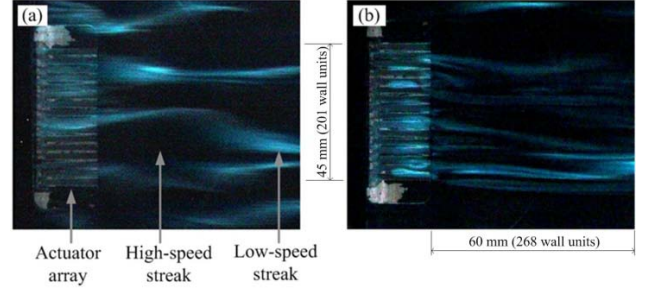


Figure 3. Typical photographs of instantaneous flow structures in the  $xz$ -plane at  $y^+ = 6.5$  from smoke-wire flow visualization: (a) uncontrolled, (b) controlled [ $A_o^+ = 1.43, f_o^+ = 1.56, \lambda_z^+ = 269$  (or  $\phi_{i,i+1} = 18^\circ$ )]. Flow at  $U_\infty = 1.5\text{m/s}$  ( $Re_\theta = 650$ ) is left to right. Normalization is based on wall variables at  $U_\infty = 1.5\text{m/s}$  in the absence of perturbation.

Figure 3 shows typical photographs of flow structures at  $y^+ = 6.5$  from smoke-wire flow visualization. The free-stream velocity was reduced to be  $U_\infty = 1.5\text{ m/s}$ . At this lower  $U_\infty$ , the boundary layer without control remains to be turbulent, as is evident in Figure 3(a). The high- and low-speed streaks are evident, as marked by arrows in the figure. On both sides of the low-speed streak, there is a pair of counter-rotating longitudinal vortices pumping low-momentum fluid away from the wall. Meanwhile, on the downdraught sides of the vortices, high-momentum fluid was induced to move towards the wall, thus forming high-speed streaks. High- and low-speed streaks are always side by side accompanied by each other, producing large velocity gradient and Reynolds shear stress between. The average spanwise spacing between low-speed streaks is about 100 wall units, in line with results from the hydrogen bubble flow visualization. However, once the actuators were operated at  $A_o^+ = 1.43, f_o^+ = 1.56$  and  $\lambda_z^+ = 269$  (or  $\phi_{i,i+1} = 18^\circ$ ) (Figure 3b), the large-scale streaky structures could not be seen, instead, some substantially smaller scale longitudinal structures occur, along with an increased area of low-speed region downstream of the actuator array. Apparently, there is a great change in the flow structure. The near-wall flow structure over a wall made with riblets is dominated by longitudinal vortices in pairs, which are short and have a large spanwise spacing between them, compared with those over a smooth wall [5]. The spanwise oscillating wall creates a negative spanwise vorticity near the wall, resulting in the reduced streamwise velocity in the near-wall region as the vortex sheet in the Stokes layer is tilted along the spanwise direction. The resultant velocity reduction hampers the stretching of the longitudinal vortices, weakening the sweep events [5]. As demonstrated in DNS study [8, 9], the transverse travelling wave induced by a spanwise force that is confined within the viscous sublayer suppresses the near-wall coherent structures almost completely, with the high-speed streaks disappeared in the near-wall region, similarly to the present observation. The similarity is reasonable and as a matter of fact provides a validation for the present result since both Du et al. (2002) [9] and the present

control techniques are related to a transverse travelling wave produced by actuation.

In view of the fact that  $\tau_w$  and  $u$  in the near-wall region are correlated [3, 4], the space-time cross-correlation between  $\tau_w$  and  $u$  is investigated in  $xy$ -plane. The local  $\tau_w$  at  $z^+ = 0$  and  $x^+ = 35$  was measured using the hot-film flush-mounted on the wall. While the hot-film probe was fixed on the wall, the hotwire probe to measure  $u$  was traversed from  $y^+ \approx 0$  to 20 and  $x^+ = 35$  to 310 to determine the space-time cross-correlation in the  $xy$ -plane. The traverse increment is  $(\Delta x^+, \Delta y^+) = (7, 0.7)$ .

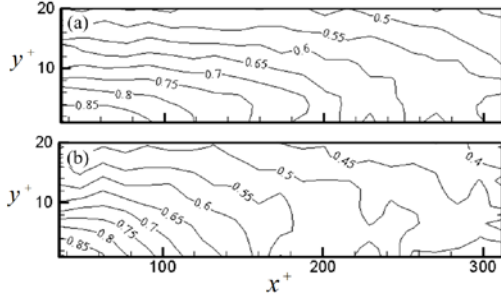


Figure 4. Iso-contours of the maximum cross-correlation coefficient  $\rho_{\tau_w u} = \overline{\tau_w(t)u(t + \tau_o)} / (\tau_{w,rms} u_{rms})$  in the  $xy$ -plane ( $z^+ = 0$ ): (a) uncontrolled, (b) controlled [ $A_o^+ = 1.94$ ,  $f_o^+ = 0.39$ ,  $\lambda_z^+ = 416$  (or  $\phi_{i,i+1} = 18^\circ$ )].  $U_\infty = 2.4$  m/s.

Figure 4 presents the iso-contours of the maximum cross-correlation coefficient, defined by  $\rho_{\tau_w u} = \overline{\tau_w(t)u(t + \tau_o)} / (\tau_{w,rms} u_{rms})$ , where  $\tau_o$  is the time-delay to obtain the cross-correlation peak, in the  $xy$ -plane with and without control. The control parameters are  $A_o^+ = 1.94$ ,  $f_o^+ = 0.39$  and  $\lambda_z^+ = 416$ , under which  $\delta_{\tau_w}$  is -35% at  $x^+ = 35$  and  $z^+ = 0$ . It is evident that the  $\rho_{\tau_w u}$ -contours contracts as a results of control. For example, the contour of  $\rho_{\tau_w u} = 0.55$  extends to beyond  $x^+ = 310$  without control (Figure 4a) but ends at  $x^+ \approx 160$ , retreating by about 50%, under control (Figure 4b). On the other hand, the contraction in the cross-stream direction is more moderate, not more than 10%. The  $\rho_{\tau_w u}$ -contours in the  $yz$ -plane (not shown) also retreat greatly in the spanwise direction, but moderately in the cross-stream direction. The observation is apparently linked to the longitudinal streaky coherent structures and perhaps also to the convective nature of these structures.

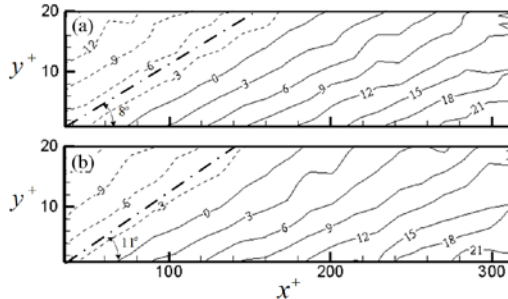


Figure 5. Iso-contours of the time-delay  $\tau_o$  (units in ms) corresponding to the cross-correlation peaks (figure 4): (a) uncontrolled, (b) controlled [ $A_o^+ = 1.94$ ,  $f_o^+ = 0.39$ ,  $\lambda_z^+ = 416$  (or  $\phi_{i,i+1} = 18^\circ$ )].  $U_\infty = 2.4$  m/s.

The iso-contours of  $\tau_o$ , which corresponds to the cross-correlation peaks with and without control in Figure 4, is presented in Figure 5. The contours appear inclined with respect to the flow direction. Since the iso-contours of  $\tau_o$  provide a good measure of the spatial structure of the coherent structure, it may be inferred that the large-scale coherent structures are forwards-inclined. As

indicated by the dotted line, the inclination angle is about  $8^\circ$ , with respect to the flow direction in the absence of control; but the angle increases to about  $11^\circ$  under control. This increase may be linked to the actuation in the wall-normal direction, which causes the flow to run away from the wall, thus pushing the coherent structure upward.

## Conclusions

Active control of a fully developed TBL ( $Re_\theta = 1,000$ ) over a flat plate has been investigated with a view to reduce skin-friction drag. The investigation leads to following conclusions.

- (i) The control performance depends strongly on  $A_o^+$ ,  $f_o^+$ , and  $\lambda_z^+$ . The maximum friction drag reduction presently observed is 50% at  $x^+ = 17$  under  $\lambda_z^+ = 416$ ,  $A_o^+ = 1.94$  and  $f_o^+ \geq 0.39$ .
- (ii) The large-scale longitudinal streaky coherent structures break up under control; their size contracts substantially, particularly along the longitudinal and spanwise directions. Meanwhile, the forwards-inclined coherent structures were pushed slightly upwards by actuations. These alterations in flow structures under control are favourably towards drag reduction.

## Acknowledgments

YZ wishes to acknowledge support given to him from Research Grants Council of HKSAR through grant PolyU 5334/06E and from The Hong Kong Polytechnic University through grant G-U394.

## References

- [1] Kim, J., Control of Turbulent Boundary Layer, *Phys. Fluids A*, **15**, 2002, 1093-1105.
- [2] Bernard, P. S., Thomas, J. M. & Handler, R. A., Vortex Dynamics and the Production of Reynolds Stress, *J. Fluid Mech.*, **253**, 1993, 385-419.
- [3] Kravchenko, A. G., Choi, H. & Moin, P., On the Generation of Near-wall Streamwise Vortices to Wall Skin Friction in Turbulent Boundary Layers, *Phys. Fluids A*, **5**, 1993, 3307-9.
- [4] Schoppa, W. & Hussain, F., Coherent Structure Generation in Near-wall Turbulence, *J. Fluid Mech.*, **453**, 2002, 57-108.
- [5] Karniadakis, G. E. & Choi, K.-S., Mechanisms on Transverse Motions in Turbulent Wall Flows, *Annu. Rev. Fluid Mech.*, **35**, 2003, 45-62.
- [6] Berger, T. W., Kim, J., Lee, C. & Lim, J., Turbulent Boundary Layer Control Utilizing the Lorentz Force, *Phys. Fluids*, **12**, 2000, 631-649.
- [7] Choi, K.-S., DeBisschop, J.-R. & Clayton, B. R., Turbulent Boundary-layer Control by Means of Spanwise-wall Oscillation, *AIAA J.*, **36**(7), 1998, 1157-63.
- [8] Du, Y. Q. & Karniadakis, G. E., Suppressing Wall Turbulence by Means of a Transverse Travelling Wave, *Science*, **288**, 2000, 1230-34.
- [9] Du, Y. Q., Symeonidis, V. & Karniadakis, G. E., Drag Reduction in Wall-bounded Turbulence via a Transverse Travelling Wave, *J. Fluid Mech.*, **457**, 2002, 1-34.
- [10] Segawa, T., Kawaguchi, Y., Kikushima, Y. & Yoshida, H., Active Control of Streak Structures in Wall Turbulence Using an Actuator Array Producing Inclined Wavy Disturbances, *J. Turbulence*, **3**, 2002, 1-15.